Fuel 383 (2025) 133834

Contents lists available at ScienceDirect

Fuel

journal homepage: www.elsevier.com/locate/fuel

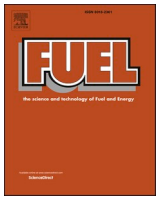

Full Length Article

Laminar burning velocity and explosion characteristics of a lignocellulose-derived bio-jet fuel at elevated pressures and temperatures

Qiyang Wang, Zhongyang Luo *, Cangsu Xu, Chunjiang Yu

State Key Laboratory of Clean Energy Utilization, Zhejiang University, Hangzhou 310027, PR China

ARTICLE INFO

Keywords:
Bio-jet fuel
Laminar burning velocity
Markstein length
Pressure oscillation

ABSTRACT

The production of aviation fuel from lignocellulose is inexpensive and has high selectivity and atom economy. The authors reproduced a mixed fuel of a bio-jet fuel candidate, which was obtained from lignocellulose using the hydropyrolysis vapor upgrading process. The combustion characteristics of this fuel have not been studied yet, so the laminar burning velocity and explosion characteristics of the fuel were investigated under a wide range of conditions in a constant volume combustion chamber at initial pressures of 1, 2, and 4 bar, initial temperatures of 400, 435, and 470 K, and equivalence ratios of 0.7–1.4. The results show that the laminar burning velocity of the fuel is maximum at the equivalence ratio of 1.1–1.2, which is close to that of RP-3 and Jet A-1 but smaller than that of bio-jet fuels produced through hydroprocessed esters and fatty acids. The simulation shows good agreement with experiment at elevated temperatures. The explosion intensity increases with an increase in the equivalence ratio under elevated initial pressures due to pressure oscillation. The dominant frequency of the pressure oscillation is slightly higher than that of the brightness oscillation, both of which are between 2500 and 3000 Hz The reduction of Markstein length is correlated with pressure oscillations and brightness oscillations.

1. Introduction

Air transportation has increasingly become important in world tourism and trade. Recently, the International Civil Aviation Organization adopted a Long-Term Aspirational Goal to achieve net zero CO_2 emissions by 2050 [1]. The industry expects sustainable aviation fuel or the so-called bio-jet fuel to play a significant role in decarbonizing aviation. As the only renewable carbon resource, biomass is considered a potential substitute for fossil fuels due to its large output, high organic content, strong sustainability, low cost, and low greenhouse gas emissions [2]. Lignocellulose is the most abundant biomass resource on earth, with an annual output of approximately 17 billion tonnes. However, humans do not use more than 5 % of the lignocellulose produced for various purposes [3]. In recent years, the direct catalytic conversion of lignocellulose into aviation fuel has attracted extensive attention due to its advantages of low raw material cost, mild reaction conditions, and high selectivity of the desired products [4,5].

Aviation kerosene is a complex mixture composed of thousands of hydrocarbons, including straight-chain alkanes, branched-chain alkanes, cycloalkanes, and aromatics. However, most bio-jet fuel is currently synthesized through the hydroprocessed esters and fatty acids (HEFA) pathway [6], and the product is mainly paraffin, lacking cycloalkanes and aromatics. While high levels of aromatics can increase soot formation, aromatics are necessary to avoid leaking fuel system seals [7]. In addition, cycloalkanes help to lower the freezing point of fuel and increase fuel density and thermal stability [8]. In this regard, lignocellulose can achieve the production of all basic components of aviation fuel, more specifically, cellulose and hemicellulose can produce paraffin, and lignin can produce cycloalkanes and aromatics, thereby achieving high atom economy [4]. This will help solve the current situation where bio-jet fuel can only be mixed with aviation kerosene for use, thereby contributing to achieving net zero carbon emissions in the aviation industry.

The urgent demand and rapid development of bio-jet fuels have attracted many researchers to study the combustion characteristics of bio-jet fuel to gain an in-depth understanding of their feasibility and impact on combustion systems. Currently, many researchers have studied the basic combustion properties of different bio-jet fuels. The flame speed of fuel is an important indicator that affects the flammability inside the combustor [9]. Laminar burning velocity (LBV) is the speed of a steady one-dimensional adiabatic free flame propagating in

* Corresponding author.
E-mail address: zyluo@zju.edu.cn (Z. Luo).

https://doi.org/10.1016/j.fuel.2024.133834
Received 10 August 2024; Received in revised form 23 October 2024; Accepted 21 November 2024
Available online 30 November 2024

Nomenclature

Symbols

c	Sound velocity of the combustion gas (m/s)
D	Diameter of the combustion chamber (m)
dp/dt	Pressure rise rate (bar·s^{-1})
$(dp/dt)_{max}$	Maximum pressure rise rate (bar·s^{-1})
$f_{m,n}$	Resonant frequency of the mode (m, n) (Hz)
K	Flame stretch rate (1/s)
L_b	Markstein length (m)
p	Pressure (bar)
p_0	Initial pressure (bar)
p_r	Reference pressure (bar)
p_{max}	Maximum Explosion pressure (bar)
p_{max}/p_0	Normalized maximum explosion pressure
r_f	Flame radius (m)
S_b^0	Unstretched flame speed (m/s)
S_b	Stretched flame speed (m/s)
S_L	Laminar burning velocity (m/s)
t	Time after ignition (ms)
t_c	Explosion time (ms)
T	Temperature (K)
T_0	Initial temperature (K)
T_r	Reference temperature (K)
u_r	Reference laminar burning velocity (m/s)

Greek Symbols

α	Temperature exponent
β	Pressure exponent
φ	Equivalence ratio
$\eta_{m,n}$	Dimensionless number of modes (m, n)
ρ_b	Density of burned gas (g/cm^3)
ρ_u	Density of unburned gas (g/cm3)

Abbreviations

13DMCH	1,3-dimethylcyclohexane
135TMB	Mesitylene
AtJ-SPK	Alcohol-to-Jet Synthetic Paraffinic Kerosene
CVCC	Constant volume combustion chamber
DEC	Decalin
HEFA	Hydroprocessed esters and fatty acids
LBV	Laminar burning velocity
NHED	n- hexadecane
TEL	Tetralin

the doubly infinite domain [10]. It can provide verification targets for chemical kinetic mechanisms, and affect combustion efficiency and emissions at a practical level. Ultimately, it contributes to engine design and optimization [11]. Hui et al. [12] measured the LBV of a camelina-derived hydroprocessed renewable jet (CHRJ) at an initial pressure of 1 bar and an initial temperature of 400 K and 470 K. The results showed that there was no significant difference between traditional jet fuel and synthetic jet fuel. In Munzar's study [13,14], certain proportions of HEFA biomass fuel were blended with Jet A-1. It was revealed that the LBV of the 20 % blending ratio of CHRJ was similar to that of Jet A-1. In addition, they emphasized the importance of obtaining accurate LBVs at high temperatures and pressures. Liu et al. [15,16] studied the LBV of two RP-3/microalgae oil mixed fuels and analyzed the influence of different microalgae oil addition ratios. The addition of microalgae oil increases the LBV of the mixed fuel and also changes the flame stability and the sensitivity of LBV to equivalence ratio and temperature. Richter et al. [17] measured the LBV and ignition delay time of AtJ-SPK and proposed a new chemical mechanism for the fuel. However, research on the combustion characteristics of bio-jet fuel produced from lignocellulose is very scarce. Xu et al. [18] obtained a bio-jet fuel candidate rich in cycloalkanes by performing hydrodeoxygenation on corn stover lignin and measured its LBV and explosion characteristics.

In addition, during fuel processing, storage, transportation, and use, explosions may occur when leaked or spilt fuel forms a combustible mixture with air and encounters a strong ignition source [19]. Explosion parameters are also beneficial for assessing combustors performance. Zhang et al.[20] used n-hexane as a surrogate fuel for aviation kerosene and studied the effect of different initial temperatures and pressures on the explosion characteristics of n-hexane in a cylindrical container. They found that the maximum explosion pressure and maximum pressure rise rate increased with the increase of initial pressure and the decrease of initial temperature. In their subsequent study [21], they explored the effect of hydrogen addition on the explosion characteristics of n-hexane. Xu et al. [22] used n-decane as a surrogate fuel for aviation kerosene and studied the effect of hydrogen addition on its explosion characteristics. However, research on the explosion characteristics of bio-jet fuel remains insufficient. Recently, the author's team prepared a bio-jet fuel candidate through the hydropyrolysis vapor upgrading process of lignocellulose [23]. Poplar wood was used as the biomass raw material. The fuel calorific value is 46.2 MJ/kg. More detailed process of fuel production can be seen in [23]. It should be noted that the composition of this fuel is higher in cycloalkanes, lower in alkanes, and has similar levels of aromatic hydrocarbons compared to conventional jet fuels. The GCMS spectrum and detailed compositional information can be found in the Supplementary Material. A mixed fuel was build composed of 54 % 1,3-dimethylcyclohexane (13DMCH), 9 % n- hexadecane (NHED), 12 % mesitylene (135TMB), 10 % tetralin (TEL) and 15 % decalin (DEC) in mole ratio was reproduced using standardized methods [24]. The fuels involved in the mixed fuel are typical components of aviation kerosene or automotive oil, and are supported by corresponding chemical kinetics research [25–27].

Generally, bio-jet fuel would be beneficial to realize carbon neutrality in the aviation industry. Although lignocellulose-derived bio-jet fuel is a promising aviation fuel due to its low cost, high selectivity, and high atom economy, and also contains aromatics and cycloalkanes, there is a lack of research on its combustion and explosion characteristics. In this work, in order to investigate the effects of different initial temperatures and pressures on the combustion characteristics of lignocellulose-derived bio-jet fuel at different equivalence ratios, the laminar burning velocity and explosion characteristics have been experimental studied in a constant volume combustion chamber at the initial pressures of 1, 2 and 4 bar, the initial temperatures of 400, 435 and 470 K, and the equivalence ratios of 0.7–1.4, with an interval of 0.1. And the developed reaction mechanism was used to simulate the laminar burning velocity. This work will be beneficial for the application of lignocellulose-derived bio-jet fuel in engines and the safety of production and use processes.

2. Experimental and data processing specifications

2.1. Experimental setup

Fig. 1 shows a schematic diagram of the experimental setup used in this study, where the constant volume combustion chamber (CVCC) was self-made by the author and its verification can be found in the Supplementary Materials. The system consists of a constant volume combustion chamber, a high-speed Schlieren photography system, a pressure acquisition system, an ignition control system, a heating system, and intake and exhaust system. The CVCC is an octagonal prism with an outer surface coated with insulation paint, and each side has a

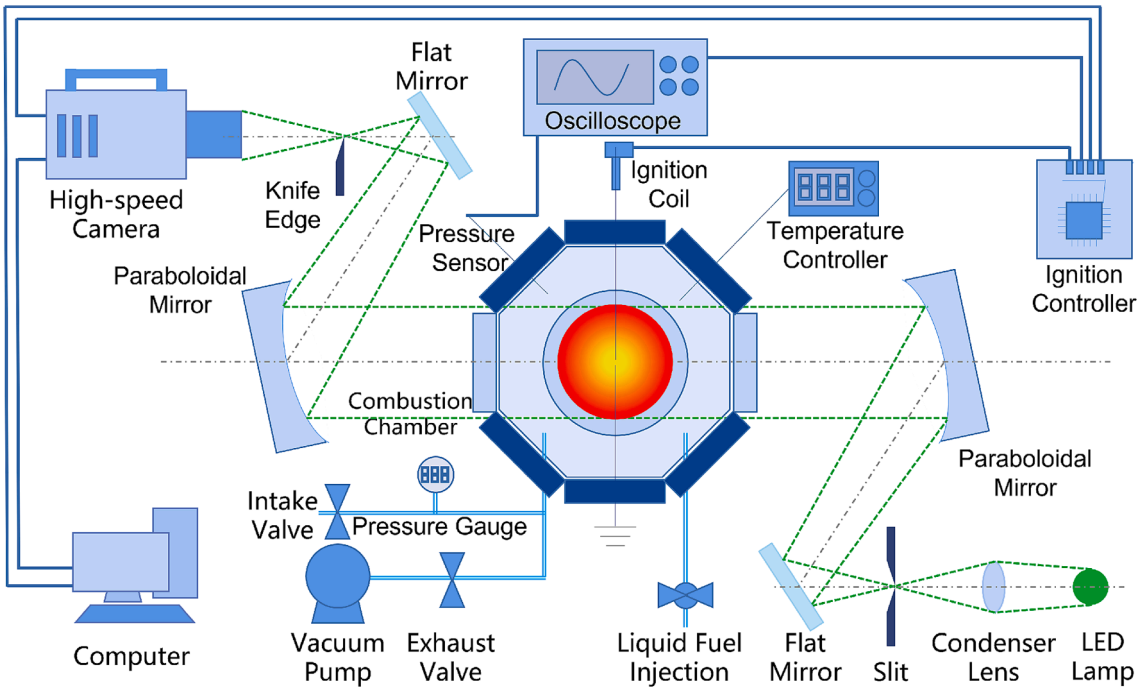

Fig. 1. Experimental setup.

window. Its inner cavity is approximately composed of a cylinder and its volume is 17.1 L. 132 heating rods with a rated power of 60 W are evenly distributed in the reserved holes of the CVCC. The K-type thermocouple is used to measure the initial temperature and is heated to the set temperature through a temperature controller. The pressure sensor (CY-YD-200, SINOCERA PIEZOTRONICS, INC.) with the natural frequency of 75 kHz is used to measure the pressure rise during the combustion process and record it through an oscilloscope, and a high-precision pressure gauge is used to measure the initial pressure. A pair of quartz glass with a diameter of 105 mm is installed on two sides of the CVCC to provide optical access. The vacuum pump flushes the CVCC before the mixture is injected to prevent residual combustion products from affecting the next test. Two opposing electrodes of diameters 0.8 mm are used to provide spark ignition with an ignition controller, and the ignition energy is about 15 mJ. The ignition controller sends a synchronous signal to control the high-speed camera (X213M, HF Agile Device Co., Ltd.) and oscilloscope to record the flame image and pressure data during combustion. The high-speed camera recorded the flames at a shooting speed of 10,000 frames per second and a resolution of 1280 × 1024 pixels. The detailed experimental steps can be found in previous research [28]. The experimental validation is available in previous research [29–31].

2.2. Data processing

The flame images were processed by Python code. As shown in Fig. 2, after adjusting the grayscale of the original image, the background is subtracted, the image is rotated 45° to eliminate the interference of electrode wires, and the CANNY algorithm is used for edge detection. The identified edge is enclosed with the smallest rectangle, the center of the rectangle is defined as the center of the circle, and the average of the rectangle's length and width is represented as the radius.

According to Bradley's theory [32], LBV can be obtained by flame propagation. Therefore, the time-evolution of the flame radius $r_f(t)$ is extracted frame per frame. Hence, the stretched flame speed is

$$S_b = dr_f/dt \tag{1}$$

where S_b is the stretched flame speed, and t is the time after ignition. $r_f - t$ data were smoothed by the Savitzky-Golay algorithm.

For a spherical flame, the flame stretch rate K is defined by Eq. (2).

$$K = 2S_b/r_f \tag{2}$$

Subsequently, the stretch effect could be extracted by plotting S_b versus K and the unstretched flame speed S_b^0 can be extrapolated by the linear method in Eq. (3) or the nonlinear [33] method in Eq. (4).

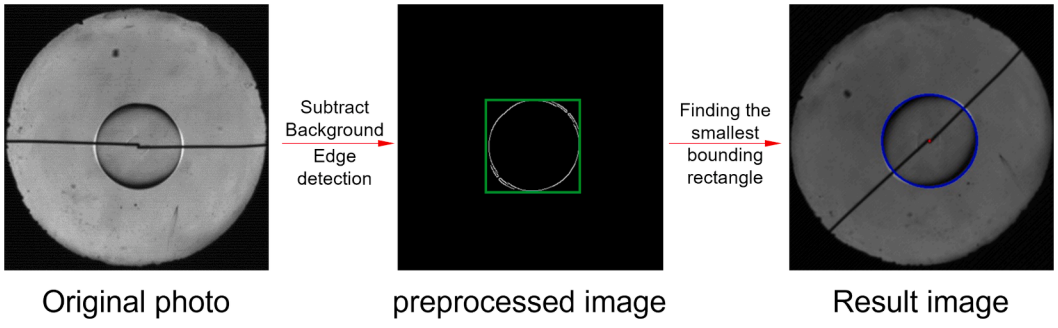

Fig. 2. Schlieren image processing.

$$S_b^0 = S_b - L_b K \tag{3}$$

$$\left(S_b/S_b^0\right)^2 ln\left(S_b/S_b^0\right)^2 = -2L_b K/S_b^0 \tag{4}$$

where L_b is the Markstein length.

Fig. 3 shows the extrapolation of unstretched flame speed using linear and nonlinear methods under lean and rich combustion conditions. Due to the influence of ignition and chamber wall confinement, a radius of 8 ~ 25 mm is selected for the fitting. For high-pressure rich burning flames, the fitting range is reduced to 8 ~ 16 mm because of the influence of flame self-acceleration. In addition, the linear method flame speed is larger than the nonlinear method speed under in lean mixture, up to 7 %, while it is almost the same in a rich mixture. However, due to the assumption of weak stretching, linear methods are not suitable for strong stretching and unequal diffusion flames [35]. In this experiment, the nonlinear method is chosen to obtain the unstretched flame speed.

The laminar burning velocity S_L can be calculated by the law of conservation of mass by Eq. (5).

$$S_L = S_b^0 \rho_b / \rho_u \tag{5}$$

where ρ_b and ρ_u are the density of burned gas and unburned gas, respectively, and they are obtained by CANTERA.

Explosion time (t_c), maximum explosion pressure (p_{max}), and maximum pressure rise rate ($(dp/dt)_{max}$) are important explosion characteristic parameters obtained from Fig. 4. The pressure curve was smoothed by the Savitzky-Golay algorithm. It is worth noting that the pressure curve exhibits significant pressure oscillations. This will cause the filtered maximum explosion pressure within the oscillating pressure deviation. Here, we adjust the threshold of the filter so that the oscillating pressure is evenly distributed on both sides of the filter pressure, as shown in the Fig. 4. The oscillation pressure is obtained by subtracting the filtered pressure from the original pressure, and the maximum value is taken as the oscillation intensity.

2.3. Modelling of laminar burning velocity

The chemical kinetic mechanism of 13DMCH and 135TMB is from Eldeeb [25] and Diévart [26], respectively. The chemical kinetic mechanism of DEC, TEL and NHED is CRACK [27]. All mechanisms are simplified through the widely used DGR method with target of LBV and then merged. The merged mechanism has 187 species and 1817 reactions. The merging mechanism was tested using the LBV of 13DMCH,

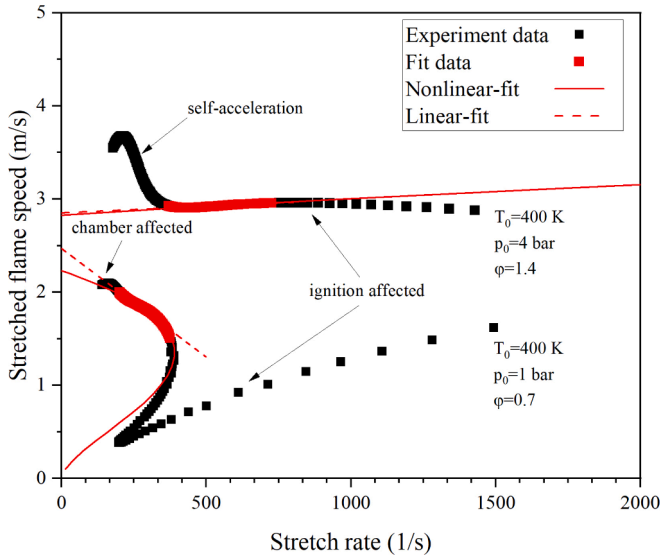

Fig. 3. Select experimental data for extrapolation.

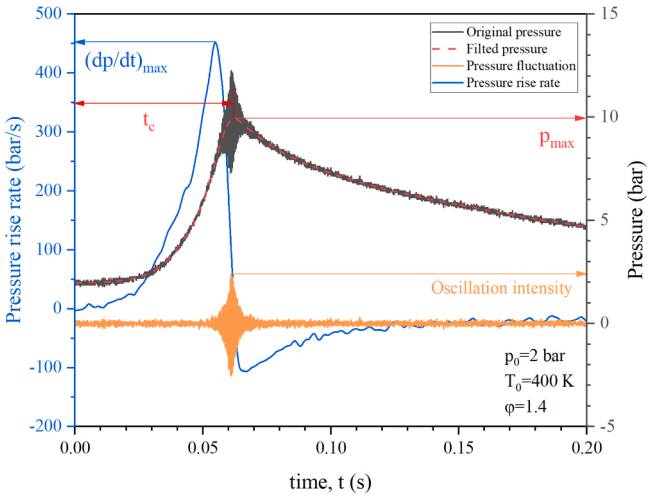

Fig. 4. Definition of explosion characteristics.

and the experimental results were in good agreement with the simulation results as shown in Fig. 5.

2.4. Uncertainty analysis

The experimental system errors are caused by the uncertainty of the initial temperature (ΔU_T), initial pressure (ΔU_P), mixture equivalence ratio (ΔU_F), number of pixels in the flame front (ΔU_A) and pressure measurement (ΔU_M). The deviation of the initial temperature control at the target temperature is ± 2 K, with a maximum ΔU_T of 0.5 %. The deviation of the initial pressure control at the target pressure is ± 0.02 bar, so ΔU_P no more than 2 %. The uncertainty of the equivalence ratio is mainly caused by fuel injection. The fuel is measured using a glass syringe with a capacity of 100 μL and a resolution of 2 μL, so ΔU_F is less than 3.5 %. For the measurement of LBV, the pixel error within the flame front in the Schlieren images was approximately ± 4 pixels, resulting in ΔU_A of approximately 1.0 %. In summary, the uncertainty of LBV ($\sqrt{(\Delta U_T)^2 + (\Delta U_P)^2 + (\Delta U_F)^2 + (\Delta U_A)^2}$) is within 4.2 %. As for the measurement of explosion characteristics, the pressure measurement error is due to filtering which is controlled within 3 %. Hence, the uncertainty of

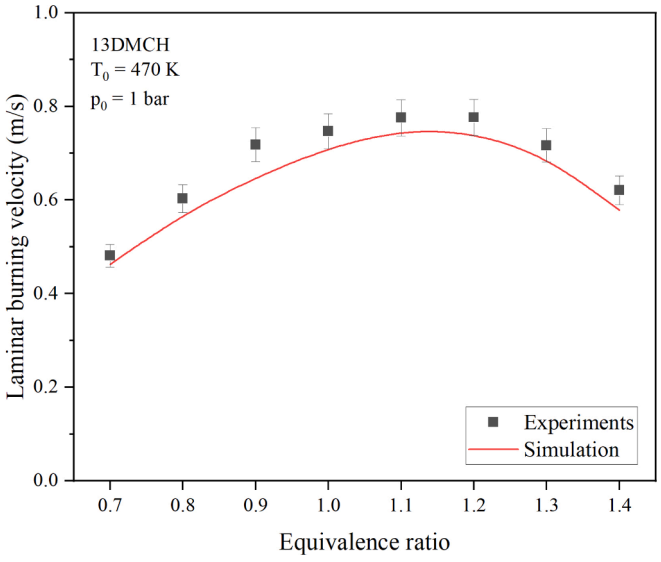

Fig. 5. Comparison between simulated LBV of merging mechanism and experimental results.

explosion characteristics ($\sqrt{(\Delta U_T)^2+(\Delta U_P)^2+(\Delta U_F)^2+(\Delta U_M)^2}$) is within 5.1 %. In addition, the experiments of each working condition were repeated 3 times, and the results were averaged to eliminate random errors.

3. Results and discussion

3.1. Flame morphology

Fig. 6 shows the flame morphology under different initial temperatures and pressures. The images from left to right correspond to flame radii of 10 mm, 20 mm, and 30 mm, and the post-ignition time is marked above. Under most initial conditions, the flame surface is smooth, but at elevated pressure and rich mixture, cracks or even cellular structures appear on the flame surface. In addition, the flame propagation speed decreases with increasing pressure in the lean mixture and at the equivalence ratio of 1, but at the rich mixture, cellularization is observed and the propagation velocity also increases. This is due to the self-acceleration phenomenon caused by the cellularization of the flame [34].

3.2. Laminar burning velocity

Fig. 7 shows the variation of LBV under various initial conditions. The LBV first increases and then decreases, reaching the maximum value at the equivalence ratio of 1.1 ~ 1.2. In addition, the LBV increases with increasing temperature because of enhanced chemical reaction rate. As the pressure increases, LBV decreases due to an increase in burnt density as the initial pressure increases. Three-body chain termination reactions are also enhanced with the increase in pressure, the concentration of free radicals in the flame decreases, and ultimately the LBV decreases [10]. The curve displays the results of simulations. The simulation results are smaller than the experimental results and the maximum difference between the experimental and simulated results is no more than 20 %, and the average is about 10 %, which is within the normal range. In a high-temperature environment at 1 bar, the simulation results are closer to the experiment, while in high-pressure rich combustion conditions, the deviation is larger. Similar situations have appeared in the literature [30]. On the one hand, unstable combustion is not considered in the simulation. On the other hand, the original mechanism is constructed at atmospheric pressure, and its prediction of pressure has not been fully verified. Further optimization of the mechanisms of the mixed fuel and its monomers are needed to achieve better prediction of experimental LBV.

The LBV was compared with other aviation kerosene and alternative fuels in Fig. 8 at an initial temperature of around 470 K and an initial pressure of 1 bar. The LBV of the fuel ranges between the LBV of RP-3 and Jet A-1 when the equivalence ratio is less than 1.1 but is higher than that of RP-3 and Jet A-1 when it is richer. Also, it is significantly smaller than CHRJ because the fuel produced using HEFA is mainly composed of alkanes, which have higher reactivity than cycloalkanes of the same scale [36]. This result is similar to the results of Xu et al. [18], but due to its high proportion of oxygen-containing compounds, it has a slightly lower LBV compared to this experiment.

The quantitative impact can be calculated through the widely used

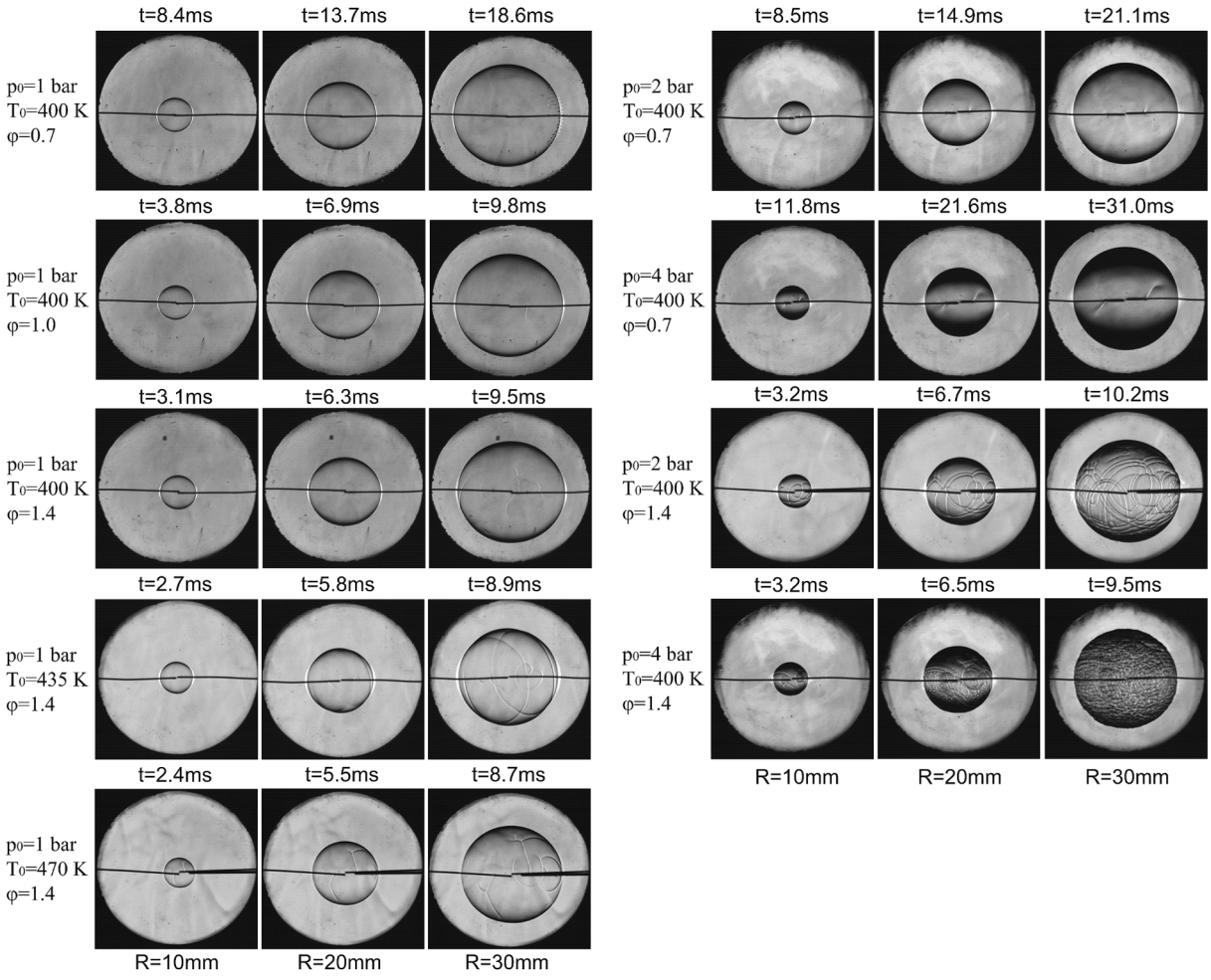

Fig. 6. Flame schlieren images under different initial temperatures and pressures.

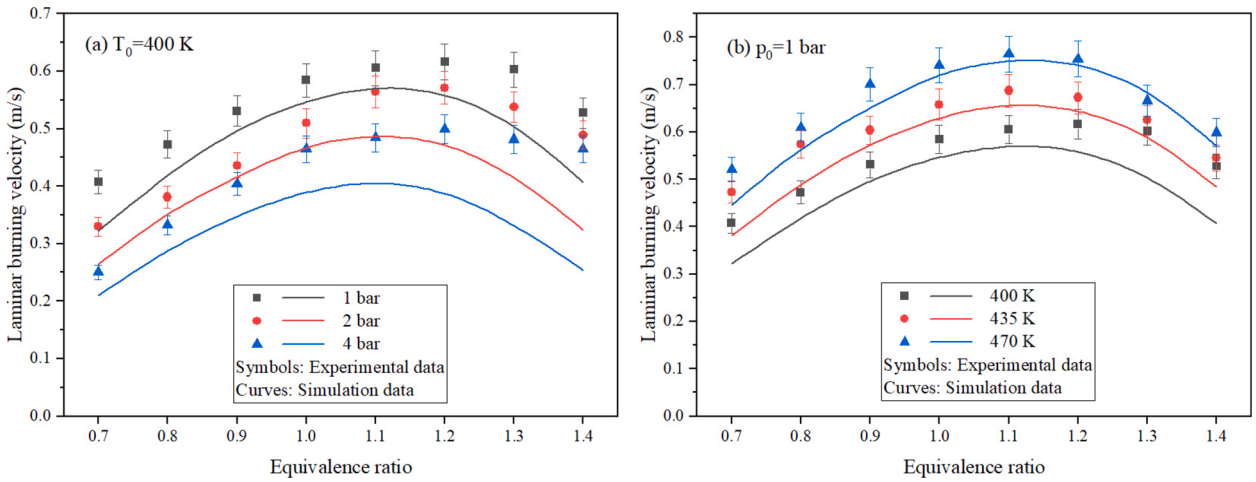

Fig. 7. Laminar burning velocity of the fuel under different (a) initial pressures and (b) initial temperatures.

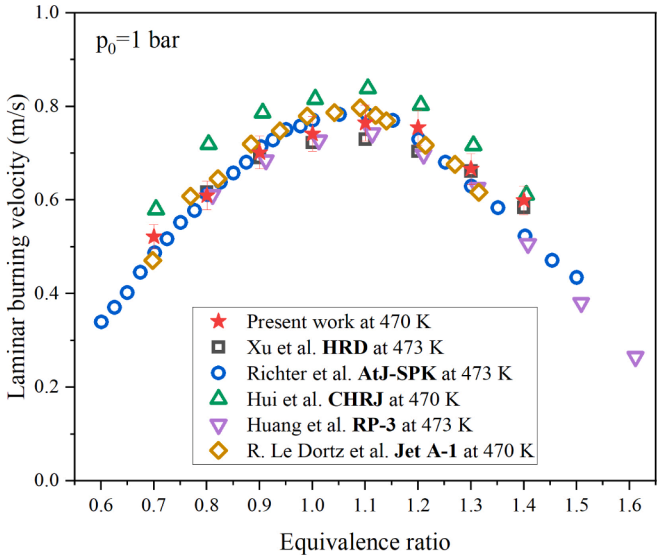

Fig. 8. Comparison of LBV of the mixed fuel, traditional aviation kerosene, and biomass alternative fuels. Xu et al. [18], Richter et al. [17], Hui et al. [12], Huang et al. [37], R. Le Dortz et al. [38].

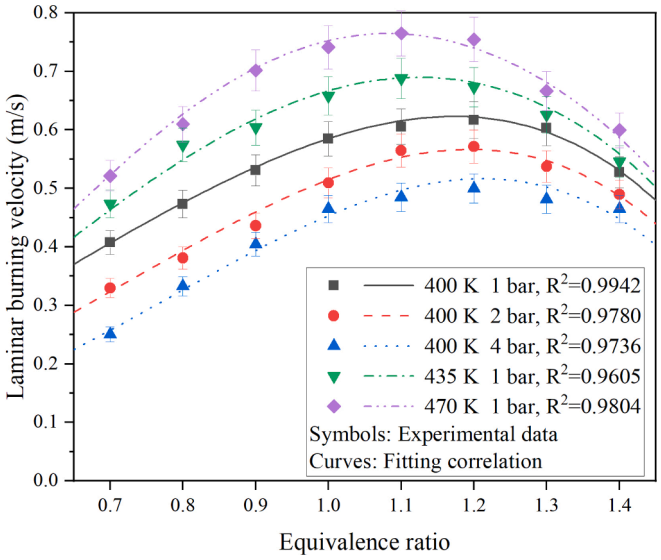

Fig. 9. Comparison of the fitting correlation (curves) with the experimental data (symbols) for the fuel.

power-law correlation by Eq. (6), where u_r is the reference LBV, T_0 (400 K) and p_0 (1 bar) are the reference temperature and pressure, respectively. α and β are the temperature and pressure exponents, respectively. A 12-term burning velocity correlation shown in Eqs. (6)–(9) can be used to describe the dependence of LBV on temperature and pressure [39]. As the results shown in Table 1 that temperature index α always positive, indicating that temperature has a promoting effect on LBV. On the contrary, the pressure index β always negative, indicating that increasing pressure will slow down LBV. Fig. 9 compares the fitted curves with the experimental data, demonstrating the significant consistency between them. The maximum deviation between the fitting correlation and experimental data is 5.39 %, and the average deviation is 1.86 %.

Table 1
Correlation coefficients and exponents of Eq. (8) for the fuel.

Equivalence ratio (φ)	u_r values (m/s)	α values	β values
0.7	0.407	1.578	−0.338
0.8	0.473	1.705	−0.269
0.9	0.531	1.694	−0.218
1.0	0.585	1.46	−0.173
1.1	0.605	1.465	−0.146
1.2	0.617	1.211	−0.142
1.3	0.603	0.585	−0.163
1.4	0.527	0.717	−0.095

$$S_L = u_r (T/T_0)^{\alpha} (p/p_0)^{\beta} \tag{6}$$

where

$$u_r = 0.585 + 0.406(\varphi - 1) - 0.895(\varphi - 1)^2 - 1.001(\varphi - 1)^3 - 0.390(\varphi - 1)^4 \tag{7}$$

$$\alpha = 1.561 - 1.890(\varphi - 1) - 4.081(\varphi - 1)^2 + 7.422(\varphi - 1)^3 \tag{8}$$

$$\beta = -0.184 + 0.343(\varphi - 1) - 0.470(\varphi - 1)^2 \tag{9}$$

3.3. Explosion characteristic

Maximum explosion pressure quantifies the energy distribution of combustion propagating waves. Therefore, it can be used to determine the heat energy from the explosion. It has been found that the maximum explosion pressure increases proportionally with the increase of initial

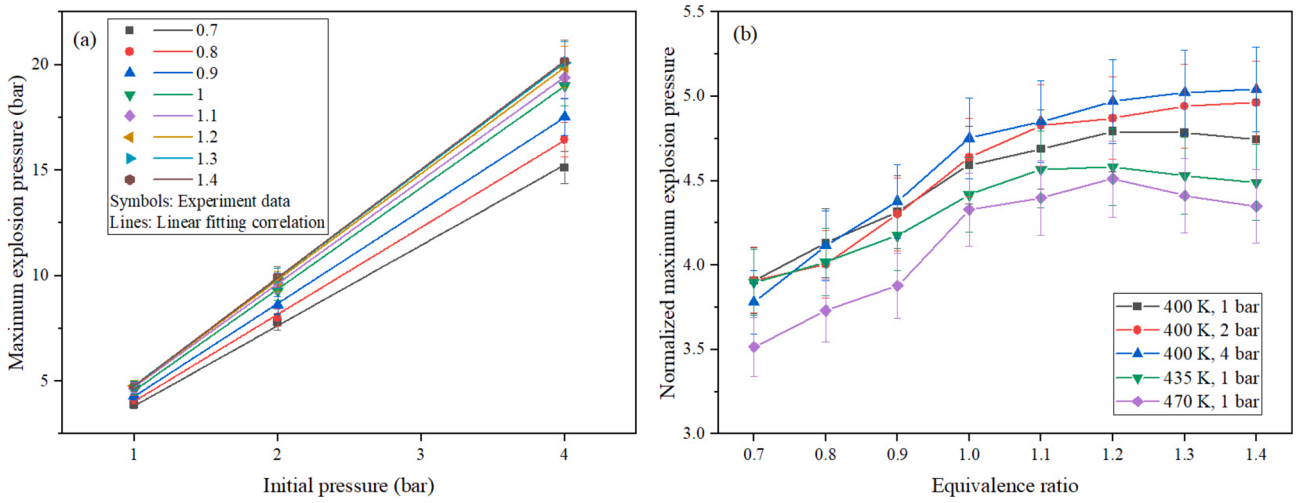

Fig. 10. (a) The variation of maximum explosion pressure with initial pressure under different equivalence ratios, (b) The variation of normalized maximum explosion pressure with equivalence ratios.

pressure as shown in Fig. 10 (a). The R^2 values of the fitting are no less than 0.99. This phenomenon has been confirmed in literature [40–42] studying different fuels, and is believed to be caused by the corresponding increase in fuel content and heat release with the increase of initial pressure. In addition, the increased pressure will intensify the collision of gas molecules, promoting the progress of the reaction [20]. It is worth noting that the slope of the fitting increases with the increase of equivalence ratio, indicating that the influence of initial pressure is amplified with the increase of equivalence ratio. Obviously, this linear relationship is conducive to predicting the combustion characteristics of any equivalence ratio of the fuel at different temperatures and pressures, which is very helpful for engine design and leakage risk assessment.

To facilitate the comparison of explosion pressures under different pressures, the explosion pressures are normalized and shown in Fig. 10 (b). At 1 bar, the explosion pressure first increases and then decreases with the increase in the equivalence ratio, attaining the maximum value at 1.1 ~ 1.2, and decreases with the increase in temperature. This is because an increase in temperature will reduce the overall amount of fuel in the CVCC, resulting in a decrease in the total heat release and the maximum explosion pressure [22]. In addition, an equivalence ratio that is too rich or too lean will inhibit complete combustion and result in a decrease in total heat release. It is worth noting that the increase in equivalence ratio and pressure acting alone have different effects from their combined effects. On the one hand, under high initial pressure, the maximum pressure increases with the increase in equivalence ratio, which is different from the case of low initial pressure. On the other hand, the normalized maximum explosion pressure under high pressure is similar or even smaller during lean combustion. As the equivalence ratio increases, the normalized explosion pressure is significantly greater than that of 1 bar. Similar phenomena have been observed in the literature [43]. By observing flame images and pressure sensor data, it was found that when both high pressure and rich combustion conditions are met simultaneously, flame cellularity and pressure oscillations will occur, resulting in a significant increase in the intensity of the explosion [44]. Therefore, additional attention needs to be paid to the effect of a significant increase in combustion intensity due to an increase in initial pressure and equivalence ratio.

The explosion time describes the time to obtain maximum explosion pressure, which is critical in the safety assessment and design of incinerators. Fig. 11 shows the explosion time under different initial conditions. In most cases, the explosion time decreases with increasing temperature and increases with increasing pressure. This is because initial temperature and pressure change the burning velocity, causing a change in the time for the fuel to fully react. However, the effect of

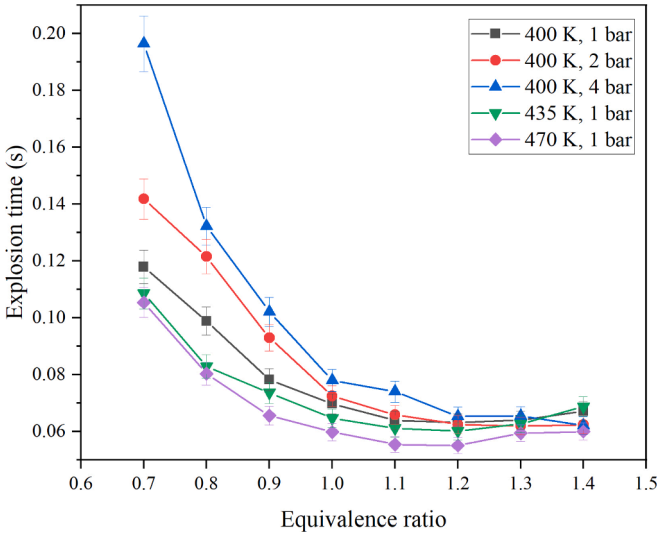

Fig. 11. Explosion time under different initial conditions.

equivalence ratio varies under different pressures. The explosion time decreases with the increase of the equivalence ratio when the equivalence ratio less than 1.1. When the initial pressure is 1 bar, it reaches the minimum value when the equivalence ratio is between 1.1 and 1.2, and then increases with the increase in the equivalence ratio. However, at elevated pressure, the explosion time decreases as the equivalence ratio increases. This is because cellularization of the flame during rich combustion accelerates the flame speed and the process of reaction.

The maximum pressure rise rate reflects the pressure accumulation during the fuel explosion process. The maximum pressure rise rate as shown in Fig. 12 has the same trend with maximum explosion pressure, and due to the proportional increase in maximum explosion pressure with the initial pressure, while the explosion time remains at a similar level, maximum pressure rise increases significantly with the increase in initial pressure. In addition, during high-pressure rich combustion, the explosion time decreases with the increase of equivalence ratio, which leads to a continuous increase in the maximum pressure rise rate. Although the total heat release is reduced at this time, the pressure can be concentrated and released, reducing heat loss and maintaining the maximum explosion pressure at a high level shown in Fig. 10 (b). However, the maximum pressure rise rate increases slightly as the

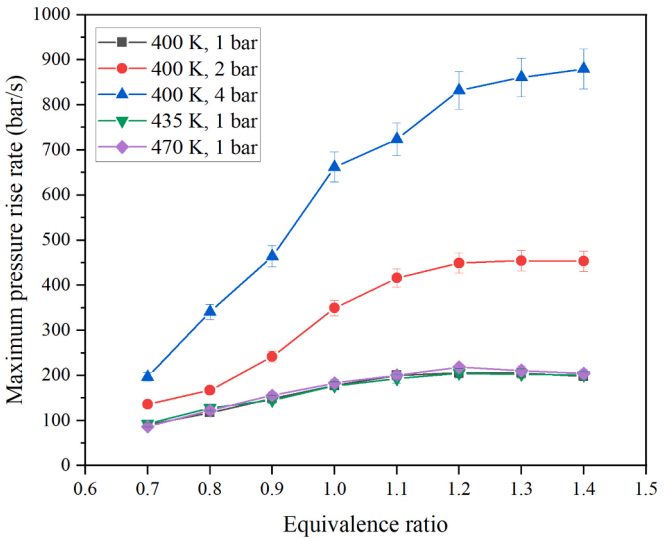

Fig. 12. Maximum pressure rise rate under different initial conditions.

temperature increases.

3.4. Pressure fluctuations

Pressure fluctuation is one of the evaluation indicators of explosion characteristics, as it often occurs in combustion. This is induced by flame instability, leading to a sudden increase in pressure and explosion severity [45]. Fig. 13 is a typical diagram of pressure oscillation with the change of equivalence ratio, showing the variation of the original pressure data when the initial pressure is 2 bar. It can be observed that the location where pressure oscillations occur is near the peak of explosion pressure, and the condition where it occur is when the equivalence ratio is greater than or equal to 1.0. From an equivalence ratio of 1.0 to 1.2, pressure oscillations significantly increase and remain at a high level between equivalence ratios of 1.2–1.4.

What is more, it was found that under certain conditions where pressure oscillations occur, the flame images may appear in a state of flicker. To describe this phenomenon, the average grayscale of the window pixels was extracted as the image brightness, and the changes in pressure were compared on the same timeline. It should be noted that in order to eliminate the initial brightness difference in each experiment, the flame image needs to be subtracted from the background image when not ignited as the brightness result. In addition, since the window only occupies a part of the photo, only the part inside the window is taken for calculation to avoid dilution of brightness by information outside the window. Fig. 14 shows the changes in pressure, flame image and brightness with time under the initial condition of 400 K and 2 bar. Due to the drastic changes in the density gradient of the cell and flame front, the brightness drops to the extremely small value point t_1. At this point, the cellular flame front just reaches the edge of the window. Afterwards, the influence of the flame front is excluded, and the brightness enters a relatively flat period. At t_2, the flame front propagates to the wall, and the flame cannot maintain a spherical structure, gradually evolving into turbulence, causing the cell structure to be destroyed and the brightness to decrease like the image shown at t_3 and t_4. Images with time greater than 79.7 ms were not recorded, but it is expected that the brightness will gradually decrease as the combustion ends.

The brightness oscillates near the pressure oscillation and they all occur during the stage of fully cellular flames, which can be observed from the images corresponding to t_3 and t_4 with alternating light and dark. Flame emission mainly comes from blackbody radiation of soot and chemiluminescence of free radicals, both of which are directly related to temperature, and under constant volume condition, temperature and pressure are directly related, hence pressure oscillations cause local temperature changes, resulting in brightness oscillations [46]. The brightness oscillation curve is obtained by the same method as the pressure oscillation. It should be noted that under all current operating conditions, brightness oscillations were only found under the condition of an equivalence ratio of 1.4 at 2 bar and 4 bar. Considering that brightness oscillations occur in rich combustion conditions, where the unburned soot content in the flame is high and there are sufficient blackbody radiation particles, while the concentration of free radicals is low in rich combustion, it is inferred that the brightness of oscillations mainly comes from the blackbody radiation of soot.

Fig. 15 shows the oscillation intensity under different initial conditions, which can be used to determine the occurrence of pressure oscillation. As the pressure increases, the equivalence ratio of pressure oscillations occurrence significantly advances and the intensity of

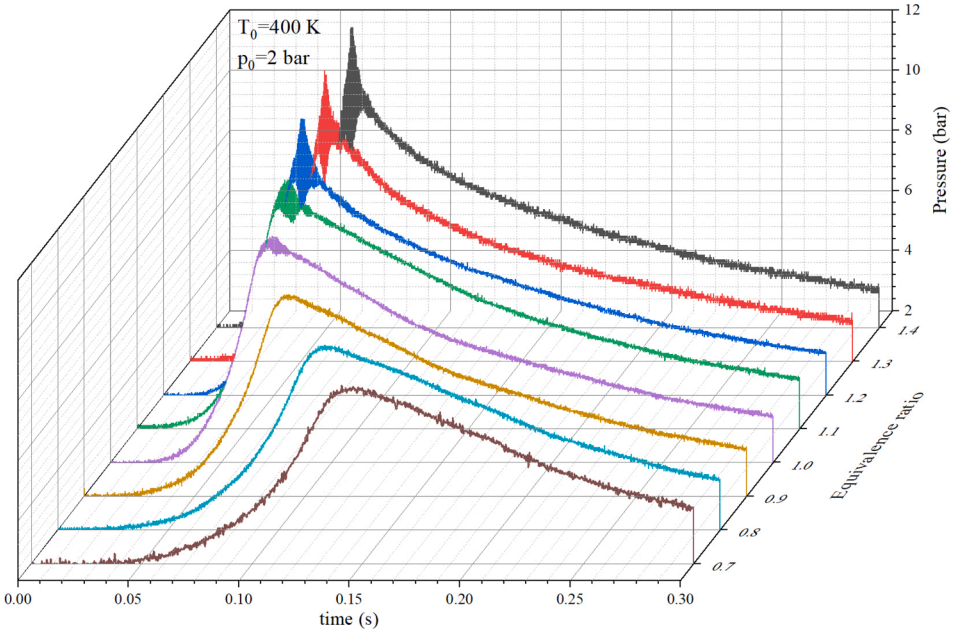

Fig. 13. Pressure oscillation with the change of equivalence ratio.

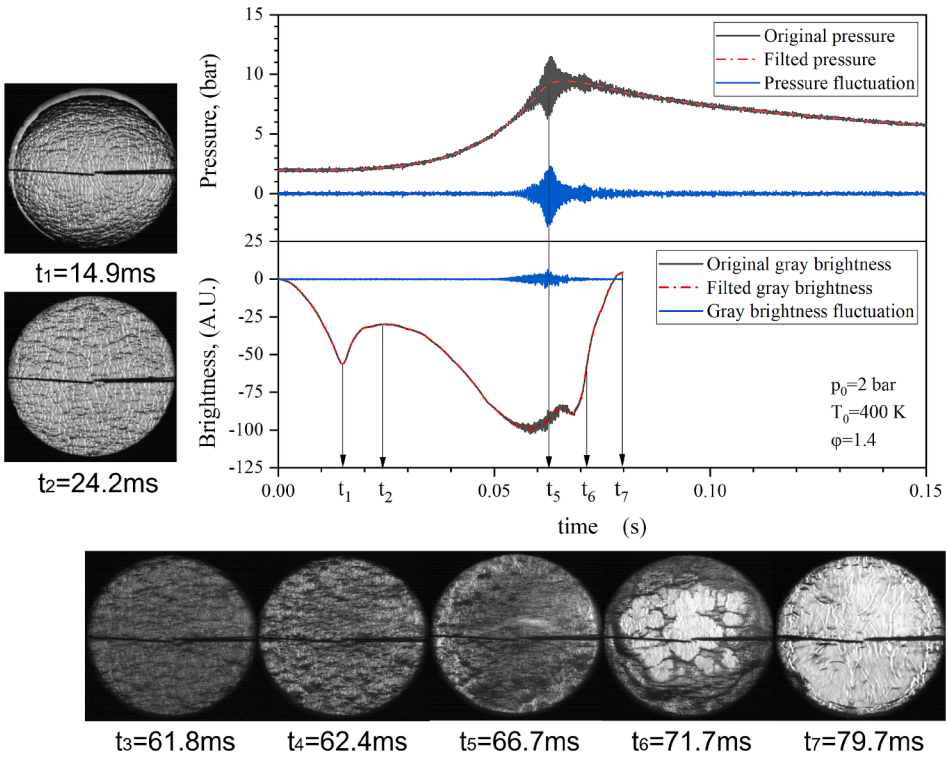

Fig. 14. Changes in pressure, brightness, and image over time.

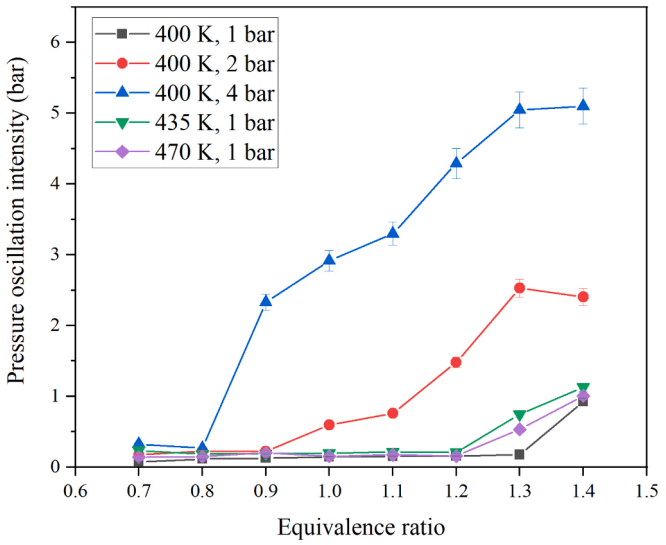

Fig. 15. Pressure oscillation intensity under different initial conditions.

oscillations increases. Also, the oscillation intensity generally increases with the increase in equivalence ratio. The increase in temperature causes oscillation to occur earlier but has slight effect on the intensity of oscillation. During high-pressure rich combustion, the oscillation intensity is significantly enhanced compare to other condition, which is consistent with the aforementioned reduction in explosion time, increase in maximum explosion pressure and maximum pressure rise rate.

A deep understanding of the modes of pressure oscillations in combustion systems is crucial for safety, as thermal-acoustic excitation is often observed, which may lead to strong resonance and combustion instability [47]. Fig. 16 shows the frequency domain results of pressure oscillations and brightness oscillations obtained by Fast Fourier Transform. The dominant frequencies of brightness oscillation and pressure oscillation are both between 2500 Hz and 3000 Hz. The dominant frequency of pressure oscillation is greater than the dominant frequency of brightness oscillation. This is consistent with the conclusion in the literature [48].

According to the theory of gas oscillation in a cylindrical cavity, the frequency of the resonant mode can be calculated using Eq. (10).

$$f_{m,n} = \frac{c\eta_{m,n}}{\pi D} \tag{10}$$

where $f_{m,n}$ is the resonant frequency of the mode (m, n), c is the sound velocity of the combustion gas, and D is the diameter of the combustion chamber, $\eta_{m,n}$ is the dimensionless number of modes (m, n), which can be obtained from literature [46]. Fig. 16 shows the distribution of the first five modal frequencies in pressure oscillation and brightness oscillation. There is a certain error between the theoretical and actual values of the dominant frequency. For brightness oscillations, there is a certain systematic error due to the theoretical frequency reflecting the axial mode of the cylinder, while the actual measured image is radial. For pressure oscillations, because pressure sensors can capture pressure data in all directions, they exhibit a wider frequency band containing peaks. This may also be the cause of the difference between the dominant frequency of pressure oscillation and brightness oscillation. The dominant frequency of brightness oscillation is close to (2,0). The frequency band containing the peak of pressure oscillation is between (1,0) and (0,1), and the dominant frequency is between (2,0) and (0,1).

Fig. 17 shows the dominant frequency and amplitude of the dominant frequency under different initial conditions. Overall, the amplitude of the dominant frequency of pressure oscillation increases with the increase in pressure and it is insensitive to temperature. But in this temperature range, the change in flame instability is not significant. As the equivalence ratio increases, the amplitude of the dominant frequency first increases and then stabilizes or decreases. The dominant frequency tends to shift towards higher frequencies with the increase of oscillation intensity. The dashed line represents the theoretical main frequencies of (2,0) and (0,1) under initial conditions of 400 K and 4 bar, and the experimental values are between them. Heat loss, cavity

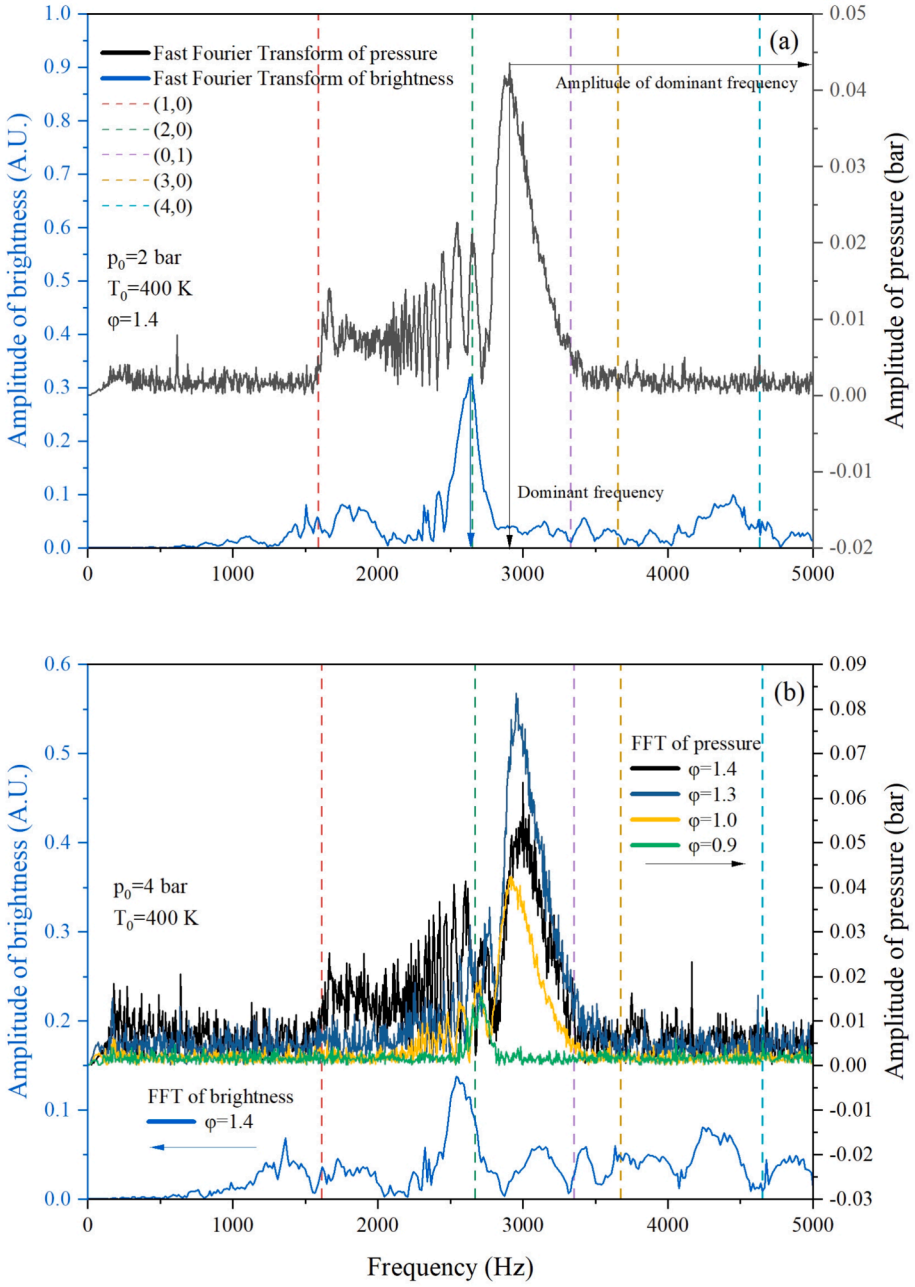

Fig. 16. Spectral analysis of pressure oscillation and brightness oscillation at an initial temperature of 400 K and initial pressure of (a) 2 bar, (b) 4 bar.

structure, and noise interference will all have an impact on the experimental values [48].

3.5. Markstein length

Combustion instability is considered the main cause of pressure oscillations [48]. Markstein length embody premixture flame susceptibility to instability or stretch influence on the flame speed. When it is negative, it represents flame instability caused by the preferential diffusion effect [29]. Fig. 18 shows the variation of Markstein length under various initial conditions. It can be seen that the Markstein length decreases as the equivalence ratio increases, indicating increasing flame instability. The Markstein length does not show a clear pattern with temperature but decreases significantly with increasing pressure. This indicates that pressure has a positive impact on thermal-diffusion instability. Under high pressure and highly rich mixture, the Markstein length is less than zero, which shows that the flame propagation speed increases with the decrease in stretch rate. Hence, small disturbances on the flame surface will be amplified, causing wrinkles on the flame surface as shown in Fig. 6.

Comparing the Markstein length with the initial conditions for pressure oscillation, it is found that when the Markstein length is less than about 0.5 mm, pressure oscillation occurs and the initial condition for the occurrence of brightness oscillation is the condition where the Markstein length is less than zero. According to Fig. 16, an increase in instability will result in longer frequency bands with higher amplitudes, which means it can provide richer oscillation frequencies and trigger brightness oscillations.

4. Conclusion

This study investigated laminar burning and explosion

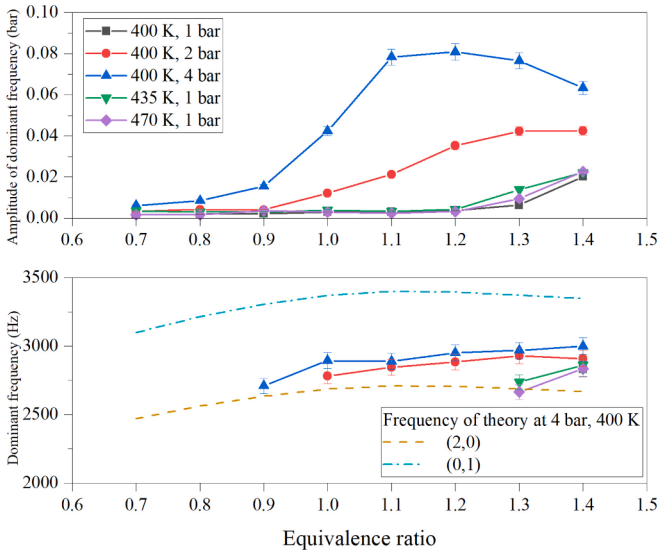

Fig. 17. Dominant frequency and amplitude of dominant frequency under different initial conditions.

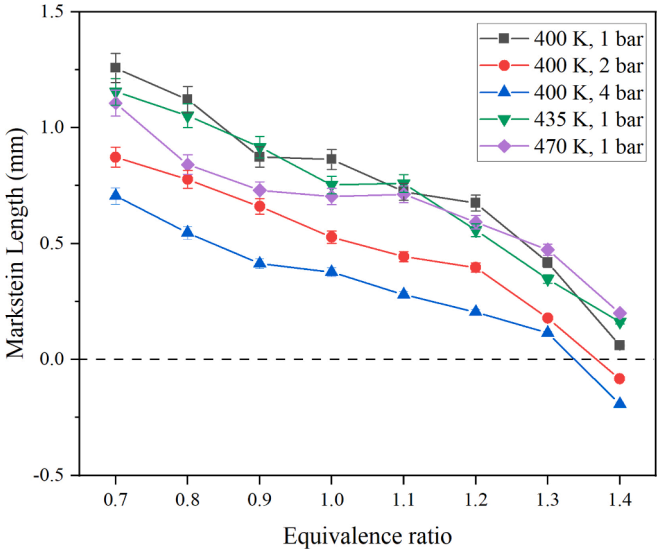

Fig. 18. Markstein length of fuel under different initial temperatures and pressures.

characteristics of a lignocellulose-derived bio-jet fuel. The main conclusions are as follows:

(1) The laminar burning velocity of the fuel first increases and then decreases with the increase in equivalence ratio, obtaining the maximum value at the equivalence ratio of 1.1–1.2. At 470 K and 1 bar, the laminar burning velocity was smaller than jet fuel produced through the HEFA process and it was between RP-3 and Jet A-1 burning velocity when the equivalence ratio was less than 1.1, but larger in rich flames.

(2) When initial pressure is 1 bar, maximum explosion pressure, and maximum pressure rise rate first increase and then decrease as the equivalence ratio increases, reaching the maximum value when the equivalence ratio is 1.1–1.2. However, under high-pressure rich combustion conditions, the explosion intensity is enhanced due to flame cellularization and pressure oscillations. The maximum oscillation intensity can reach around 5 bar.

(3) Brightness oscillation occurs when the equivalence ratio is 1.4 at elevated pressure, and the dominant frequency of the pressure oscillation is slightly higher than that of the brightness oscillation, but both are between 2500 and 3000 Hz. Also, the reduction of Markstein length is correlated with pressure oscillations and brightness oscillations.

CRediT authorship contribution statement

Qiyang Wang: Writing – original draft, Investigation, Data curation. **Zhongyang Luo:** Supervision, Project administration. **Cangsu Xu:** Writing – review & editing, Methodology. **Chunjiang Yu:** Investigation.

Declaration of competing interest

The authors declare that they have no known competing financial interests or personal relationships that could have appeared to influence the work reported in this paper.

Acknowledgements

This work was funded by the National Natural Science Foundation of China, No. 52236011.

Appendix A. Supplementary data

Supplementary data to this article can be found online at https://doi.org/10.1016/j.fuel.2024.133834.

Data availability

Data will be made available on request.

References

[1] ICAO. Long term global aspirational goal (LTAG) for international aviation. 2022. https://www.icao.int/environmental-protection/Pages/LTAG.aspx.
[2] Qiu B, Tao X, Wang J, Liu Y, Li S, Chu H. Research progress in the preparation of high-quality liquid fuels and chemicals by catalytic pyrolysis of biomass: A review. Energy Conv Manag 2022;261:115647.
[3] Zhang Z, Song J, Han B. Catalytic transformation of lignocellulose into chemicals and fuel products in ionic liquids. Chem Rev 2017;117(10):6834–80.
[4] Wang H, Yang B, Zhang Q, Zhu W. Catalytic routes for the conversion of lignocellulosic biomass to aviation fuel range hydrocarbons. Renew Sust Energ Rev 2020;120:109612.
[5] Cheng F, Brewer CE. Producing jet fuel from biomass lignin: Potential pathways to alkyl-benzenes and cycloalkanes. Renew Sust Energ Rev 2017;72:673–722.
[6] Shahriar MF, Khanal A. The current techno-economic, environmental, policy status and perspectives of sustainable aviation fuel (SAF). Fuel 2022;325:124905.
[7] Pires APP, Han Y, Kramlich J, Garcia-Perez M. Chemical composition and fuel properties of alternative jet fuels. BioResources 2018;13(2).
[8] Zhang X, Lei H, Zhu L, Wu J, Chen S. From lignocellulosic biomass to renewable cycloalkanes for jet fuels. Green Chem 2015;17(10):4736–47.
[9] Edwards T, Moses C, Dryer F. Evaluation of combustion performance of alternative aviation fuels. 46th AIAA/ASME/SAE/ASEE Joint Propulsion Conference & Exhibit 2010. https://doi.org/10.2514/6.2010-7155.
[10] Konnov AA, Mohammad A, Kishore VR, Kim NI, Prathap C, Kumar S. A comprehensive review of measurements and data analysis of laminar burning velocities for various fuel+air mixtures. Prog Energ Combust 2018;68:197–267.
[11] Egolfopoulos FN, Hansen N, Ju Y, Kohse-Höinghaus K, Law CK, Qi F. Advances and challenges in laminar flame experiments and implications for combustion chemistry. Prog Energ Combust 2014;43:36–67.
[12] Hui X, Kumar K, Sung C, Edwards T, Gardner D. Experimental studies on the combustion characteristics of alternative jet fuels. Fuel 2012;98:176–82.
[13] Munzar JD, Zia A, Versailles P, Jiménez R, Bergthorson JM, Akih-Kumgeh B. Comparison of laminar flame speeds, extinction stretch rates and vapor pressures of Jet A-1/HRJ biojet fuel blends. In: Proceedings of ASME Turbo Expo 2014: Turbine Technical Conference and Exposition; 2014. https://doi.org/10.1115/GT2014-25951.
[14] Munzar JD, Denman BM, Jiménez R, Zia A, Bergthorson JM. Flame speed and vapor pressure of biojet fuel blends. In: Proceedings of ASME Turbo Expo 2013: Turbine Technical Conference and Exposition; 2013. https://doi.org/10.1115/GT2013-94650.

[15] Liu Y, Gu W, Wang J, Ma H, Dong N, Zeng W. Laminar burning velocity of microalgae oil/RP-3 premixed flame at elevated initial temperature and pressure. Fuel 2022;309:122081.
[16] Liu Y, Wang J, Gu W, Ma H, Zeng W. An experiment study on the laminar burning velocity and markstein length of chlorella oil/RP-3 kerosene blends. ACS Omega 2020;5(37):23510–9.
[17] Richter S, Kukkadapu G, Westbrook CK, Braun-Unkhoff M, Naumann C, Köhler M, et al. A combined experimental and modeling study of combustion properties of an isoparaffinic alcohol-to-jet fuel. Combust Flame 2022;240:111994.
[18] Xu C, Liu K, Song Y, Cui D, Li X, Wang Q, et al. Laminar burning characteristics of bio-jet fuel candidate derived from lignocellulosic biomass. Fuel 2023;334:126719.
[19] Mitu M, Brandes E, Hirsch W. Mitigation effects on the explosion safety characteristic data of ethanol/air mixtures in closed vessel. Process Saf Environ 2018;117:190–9.
[20] Zhang L, Ma H, Shen Z, Wang L, Liu R, Pan J. Influence of pressure and temperature on explosion characteristics of n-hexane/air mixtures. Exp Therm Fluid Sci 2019;102:52–60.
[21] Zhang L, Ma H, Pan J, Shen Z, Wang L, Liu R, et al. Effects of hydrogen addition on the explosion characteristics of n-hexane/air mixtures. Int J Hydrogen Energ 2019; 44(3):2029–38.
[22] Xu C, Wang Q, Song Y, Liu K, Li X. Explosion characteristics of n-decane/ hydrogen/air mixtures. Int J Hydrogen Energ 2022;47(91):38837–48.
[23] Miao F, Luo Z, Zhou Q, Du L, Zhu W, Wang K, et al. Study on the reaction mechanism of C8+ aliphatic hydrocarbons obtained directly from biomass by hydropyrolysis vapor upgrading. Chem Eng J 2023;464:142639.
[24] Wu Z, Mao Y, Raza M, Zhu J, Feng Y, Wang S, et al. Surrogate fuels for RP-3 kerosene formulated by emulating molecular structures, functional groups, physical and chemical properties. Combust Flame 2019;208:388–401.
[25] Eldeeb MA, Jouzdani S, Wang Z, Sarathy SM, Akih-Kumgeh B. Experimental and chemical kinetic modeling study of dimethylcyclohexane oxidation and pyrolysis. Energ Fuel 2016;30(10):8648–57.
[26] Diévart P, Kim HH, Won SH, Ju Y, Dryer FL, Dooley S, et al. The combustion properties of 1,3,5-trimethylbenzene and a kinetic model. Fuel 2013;109:125–36.
[27] Ranzi E, Frassoldati A, Stagni A, Pelucchi M, Cuoci A, Faravelli T. Reduced kinetic schemes of complex reaction systems: fossil and biomass-derived transportation fuels. Int J Chem Kinet 2014;46(9):512–42.
[28] Wang Q, Song Y, Liu K, Li X, Xu C. Laminar combustion characteristics of methane/ methanol/air mixtures: Experimental and kinetic investigations. Case Stud Therm Eng 2023;41:102593.
[29] Oppong F, Zhongyang L, Li X, Xu C. Investigations on laminar premixed flame characteristics of ethyl acetate. Combust Flame 2021;230:111454.
[30] Xu C, Zhong A, Wang H, Jiang C, Sahu A, Zhou W, et al. Laminar burning velocity of 2-methylfuran-air mixtures at elevated pressures and temperatures: Experimental and modeling studies. Fuel 2018;231:215–23.
[31] Xu C, Zhong A, Li X, Wang C, Sahu A, Xu H, et al. Laminar burning characteristics of upgraded biomass pyrolysis fuel derived from rice husk at elevated pressures and temperatures. Fuel 2017;210:249–61.
[32] Bradley D, Hicks RA, Lawes M, Sheppard CGW, Woolley R. The measurement of laminar burning velocities and Markstein numbers for iso-octane–air and iso-octane–n-heptane–air mixtures at elevated temperatures and pressures in an explosion bomb. Combust Flame 1998;115(1):126–44.
[33] Kelley AP, Law CK. Nonlinear effects in the extraction of laminar flame speeds from expanding spherical flames. Combust Flame 2009;156(9):1844–51.
[34] Kwon OC, Rozenchan G, Law CK. Cellular instabilities and self-acceleration of outwardly propagating spherical flames. P Combust Inst 2002;29(2):1775–83.
[35] Chen Z. On the extraction of laminar flame speed and Markstein length from outwardly propagating spherical flames. Combust Flame 2011;158(2):291–300.
[36] Yang Y, Boehman AL, Simmie JM. Uniqueness in the low temperature oxidation of cycloalkanes. Combust Flame 2010;157(12):2357–68.
[37] Huang L, Huang S, Mao Y, Wang B, Zhu Q, Jiang R. An experimental study on the laminar burning velocities of RP-3 kerosene and its surrogate fuel at elevated pressures and temperatures. Fuel 2023;331:125844.
[38] Le Dortz R, Strozzi C, Sotton J, Bellenoue M. Evaluation of the surrogates capacity to reproduce the laminar burning velocities and the sensitivity to stretching of a commercial kerosene under constant volume combustion conditions. Fuel 2021; 287:119426.
[39] Hinton N, Stone R, Cracknell R. Laminar burning velocity measurements in constant volume vessels – Reconciliation of flame front imaging and pressure rise methods. Fuel 2018;211:446–57.
[40] Oppong F, Zhongyang L, Li X, Xu C. Investigations on explosion characteristics of ethyl acetate. J Loss Prevent Proc 2021;70:104409.
[41] Xu C, Wang H, Li X, Zhou W, Wang C, Wang S. Explosion characteristics of a pyrolysis biofuel derived from rice husk. J Hazard Mater 2019;369:324–33.
[42] Giurcan V, Mitu M, Movileanu C, Razus D, Oancea D. Influence of inert additives on small-scale closed vessel explosions of propane-air mixtures. Fire Safety J 2020; 111:102939.
[43] Oppong F, Li X, Xu C, Yuntang L, Liu Y. Investigations on methyl pentanoate-air mixtures confined explosion and cellularity. Fuel 2024;358:130137.
[44] Hu E, Tian H, Zhang X, Li X, Huang Z. Explosion characteristics of n-butanol/iso-octane-air mixtures. Fuel 2017;188:90–7.
[45] Xu C, Bao Y, Li X, Qian L, Oppong F. Pressure fluctuation and cellularization characteristics of 2-ethylfuran spherical expanding flame. Fuel 2023;349:128627.
[46] He X, Qi Y, Wang Z, Wang J, Shuai S, Tao L. Visualization of the mode shapes of pressure oscillation in a cylindrical cavity. Combust Sci Technol 2015;187(10): 1610–9.
[47] Dowling AP, Stow SR. Acoustic analysis of gas turbine combustors. J Propul power 2003;19(5):751–64.
[48] Ge R, Hu E, Ku J, Li J, Huang Z. Study on pressure oscillation characteristics in a constant volume bomb. Combust Flame 2021;229:111387.